## PAPER

Check for updates

# Amorphous *vs.* nanocrystalline calcium phosphate as efficient nanocarriers of elicitors in vineyards†

Belén Parra-Torrejón, [iD] [a] Marta Salvachúa-de la Fuente, [iD] [a]
Maria J. Giménez-Bañón, [b] Juan D. Moreno-Olivares, [b]
Diego F. Paladines-Quezada, [iD] [b] Juan A. Bleda-Sánchez, [b] Rocío Gil-Muñoz, [b]
Gloria B. Ramírez-Rodríguez [iD] *[a] and José M. Delgado-López [iD] *[a]

Nanotechnology is emerging as a potential strategy to achieve sustainable agricultural productivity and global food security. Engineered nanoparticles (NPs) are endowed with the ability to deliver active ingredients in a responsive manner, reducing the adverse environmental impacts in comparison to the conventional practices. However, the relationship between NP features (*i.e.*, size, morphology, surface charge, structure, *etc.*) and functionality has been scarcely studied so far. In this work, two types of calcium phosphate NPs were functionalized with the plant resistance-inductor methyl jasmonate (MeJ), which stimulates the production of secondary plant metabolites (*e.g.*, anthocyanins, stilbenes, and flavonols) in grapes. The properties of the resulting nanomaterials, namely, elongated apatite (Ap-MeJ) and round-shaped amorphous calcium phosphate NPs (ACP-MeJ), were studied in detail. In addition, the loading capacity, release kinetics and elicitor thermal stability of the two nanosystems were compared. The results indicated that the differences in terms of morphology, crystalline structure and surface charge did not affect the release kinetics nor the protective action offered by the NPs. However, ACP-MeJ showed much higher MeJ loading capacity than Ap-MeJ. Both types of nanomaterials exhibited similar performance in field experiments on Monastrell vineyards (*Vitis vinifera* L.). Foliar application of ACP-MeJ and Ap-MeJ (1 mM MeJ) produced wines with similar contents of anthocyanins and tannins (around 500 mg L$^{-1}$ and 1100 mg L$^{-1}$, respectively), but Ap-MeJ treatment required doubling the NP amount due to its lower MeJ adsorption capacity. Both treatments produced wines with higher tannin concentration than wines from non-treated grapes or wine treated with free MeJ at a much higher dosage (10 mM). Results highlight the potential of ACP and Ap NPs as elicitor nanocarriers enabling enhancement of the quality of wine in a more sustainable manner.

## Introduction

Nanomaterials are emerging as a new weapon to combat the challenge of plant protection and nutrition and address the inefficiencies of conventional agrochemicals *via* precision agricultural approaches.[1,2] Owing to their unique physicochemical properties and small dimensions, nanoparticles (NPs) are able to enter into plant cells and interact with intracellular organelles and various metabolites.[1,2] An ever-increasing number of studies have demonstrated the potential of engineered nanomaterials to

*[a] Department of Inorganic Chemistry, Faculty of Science, University of Granada, Granada, Spain. E-mail: gloria@ugr.es, jmdl@ugr.es*
*[b] Instituto Murciano de Investigación y Desarrollo Agrario y Medioambiental, Calle Mayor s/n. La Alberca, Murcia, Spain*
† Electronic supplementary information (ESI) available. See DOI: https://doi.org/10.1039/d3ce00185g

reduce the losses of fertilizers and pesticides and thus minimize their associated environmental damage.[1,2]

Calcium phosphate NPs, mainly nanocrystalline hydroxyapatite (Ap, Ca$_{10}$(PO$_4$)$_6$(OH)$_2$) and its transient precursor phase, amorphous calcium phosphate (ACP, Ca$_3$(PO$_4$)$_2$), are ideal nanocarriers for the controlled delivery of agrochemicals due to: i) their main composition, which is rich in plant nutrients (Ca and P), ii) biocompatibility and biodegradability, iii) pH-responsive solubility, iv) high surface-to-volume ratio and v) easy surface functionalization.[3,4] The vast majority of the studies were focused on the most thermodynamically stable phase, Ap, which is by far the most extended in the literature for medical applications.[5] It has been demonstrated the potential of Ap NPs as nanocarriers for the sustainable release of plant macronutrients, mainly phosphorus and urea, the most common source of nitrogen for field crops.[3,6–11] Ap NPs have been also functionalized with humic substances providing the

synergistic co-release of crop nutrients and stimulants.[12] A recent study demonstrated the potential of Ap NPs in promoting disease suppression.[13]

ACP NPs have been much less explored for environmental applications, most likely due to their transient nature. However, they can be stabilized with the use of organic molecules, such as citrate, which delays their rapid conversion into more stable crystalline calcium phosphate phases.[14–16] In a recent study, we demonstrated that ACP has higher loading capacity to host exogenous ions (*e.g.*, nitrate) or molecules (*e.g.*, urea) than Ap. This, along with the higher solubility at neutral or slightly acidic pH, and the more cost-effective production for industrial exploitation in agriculture make ACP an ideal candidate for the controlled delivery of agrochemicals (*e.g.*, fertilizers, pesticides, and elicitors).[17] ACP has been also recently used as nanocarriers of methyl jasmonate (MeJ), an elicitor able to stimulate plants to produce secondary metabolites (SMs), which protect plants against biotic and abiotic stresses.[18,19] It stimulates the production of low molecular mass SMs with antimicrobial activity, such as anthocyanins, stilbenes, and flavonols, in grapevines.[20,21] However, the treatment of free MeJ in fields presents several drawbacks due to its high volatility and its phytotoxicity when used at high doses.[22,23] We found that ACP NPs provided a sustainable release and protection against thermal degradation of the elicitor, ensuring activity over longer period of times. In fact, MeJ-doped ACP NPs reduced by 10 times the required dosage of the elicitor while maintaining the quality of the harvested grapes.[24,25]

However, the specific role of the NP properties in the performance (*i.e.*, loading capacity, release kinetics, protection, *etc.*) and efficiency in field experiments has not been studied so far. This work is aimed at evaluating how the properties of the NPs, and concretely the structure, morphology and surface charge, affect the efficiency in delivering and protecting the elicitor and the response of the plants with the two types of NPs: amorphous or nanocrystalline calcium phosphate (ACP-MeJ or Ap-MeJ, respectively). The two types of NPs were in-depth characterized to evaluate the impact of MeJ adsorption on the NP features, including loading capacities and release kinetics. Finally, the performance of the nanoassemblies was evaluated by means of field experiments in grapevines. Monastrell grapevines were treated with free MeJ (10 mM), ACP-MeJ and Ap-MeJ (both 1 mM MeJ). The effect of these preharvest treatments on the content of two important components of wines, *i.e.*, anthocyanins and tannins, was evaluated. While the anthocyanins are responsible for the red color and astringency and bitterness,[26] tannins play a relevant role in the organoleptic properties including wine mouthfeel, such as bitterness, hardness, dryness, astringency, structure, and body.[20,27]

# Experimental

## Materials

Sodium citrate tribasic dihydrate ($Na_3(C_6H_5O_7) \cdot 2H_2O$, ≥99.0% pure), sodium phosphate dibasic anhydrous ($Na_2HPO_4$,

≥99.0% pure), sodium carbonate ($Na_2CO_3$, ≥99.0% pure), calcium chloride dihydrate ($CaCl_2 \cdot 2H_2O$, ≥99.0% pure) and methyl jasmonate ($C_{13}H_{20}O_3$, 95%, racemic) were purchased from Sigma-Aldrich. All the solutions were prepared with ultrapure water (0.22 μS, 25 °C, Milli-Q, Millipore).

## Synthesis of ACP and Ap NPs

Amorphous calcium phosphate (ACP) NPs were synthesized following a batch precipitation protocol consisting of mixing two solutions of equal volume (A) $CaCl_2$ (0.2 M) and $Na_3(C_6H_5O_7)$ (0.2 M) and (B) $Na_2HPO_4$ (0.12 M) and $Na_2CO_3$ (0.1 M) at room temperature for 5 minutes.[14,17] After that, the precipitates were collected and repeatedly washed with ultrapure water by centrifugation (5000 rpm, 15 min, 18 °C).

Apatite (Ap) NPs were synthesized following a similar protocol consisting of mixing two solutions of equal volume (A) $CaCl_2$ (0.1 M) and $Na_3(C_6H_5O_7)$ (0.4 M) and (B) $Na_2HPO_4$ (0.12 M) and $Na_2CO_3$ (0.1 M). In this case, the NPs were aged in the same solution at 60 °C for 24 hours.[14,17] After that, the precipitates were collected and repeatedly washed with ultrapure water by centrifugation (5000 rpm, 15 min, 18 °C).

## Adsorption of methyl jasmonate on ACP and Ap NPs

150 mg of ACP or Ap was dispersed in 7 mL of ultrapure water and 15 mg MeJ was added to this solution to synthesize ACP-MeJ and Ap-MeJ, respectively. The MeJ/nanoparticle weight ratio was selected according to our previous study.[24] Then, the mixture was stirred for 24 hours at room temperature. Afterwards, the resulting ACP-MeJ or Ap-MeJ NPs were isolated from unbound MeJ by centrifugation (12 000 rpm, 15 min, 18 °C) and stored at 4 °C. Some aliquots were freeze-dried (Telstar) for further characterization.

The loading capacity ($Q_{max}$) was calculated by quantifying the MeJ released from 20 mg of ACP-MeJ or Ap-MeJ NPs in 1 mL of ultrapure water. After 72 hours of release, the supernatant was collected by centrifugation (12 000 rpm, 15 min, 18 °C) and the amount of MeJ in solution was estimated by UV-vis spectroscopy ($\lambda$ = 291 nm, Agilent Technologies, Santa Clara, CA, USA).[24] After that, the NP pellet was again dispersed in 0.4 mL of water and left for 72 hours to confirm if MeJ has been completely desorbed. We found that after 72 hours of release, MeJ was almost completely desorbed, with the absorbance ($\lambda$ = 291 nm) of the supernatant of the second cycle being close to cero (Fig. S4, ESI†).

## Characterization of ACP-MeJ and Ap-MeJ NPs

Fourier transform infrared (FTIR) spectra of Ap-MeJ and ACP-MeJ NPs, as well as naked Ap and ACP NPs, were recorded on a Tensor 27 (Bruker, Karlsruhe, Germany) spectrometer. Firstly, 2 mg of powdered sample was mixed with 200 mg of anhydrous potassium bromide (KBr). Secondly, the mixture was pressed at 5 tons into a 12 mm diameter disc using a hydraulic press (Specac). The infrared spectra were collected from 400 cm$^{-1}$ to 4000 cm$^{-1}$ at a resolution of 4 cm$^{-1}$. X-ray powder diffractograms (XRPD)

were recorded on a Bruker D8 Discover diffractometer from the Centre for Scientific Instrumentation of the University of Granada, (CIC-UGR), using Cu K$\alpha$ radiation ($\lambda$ = 1.5406 Å), from 8° to 60° (2$\theta$) with a scan rate of 40 s per step and a step size of 0.02° with an HV generator set at 50 kV and 1 mA. Transmission electron microscopy (TEM) images and selected-area electron diffraction (SAED) patterns of ACP-MeJ and Ap-MeJ NPs were acquired with a STEM FEI TALOS F200X microscope equipped with 4 Super-X SDDs (Thermo Fisher Scientific Waltham, MA, USA) of the Centre for Scientific Instrumentation of the University of Granada (CIC-UGR). To this aim, ACP-MeJ and Ap-MeJ NPs were ultrasonically dispersed in ultrapure water, and some drops of the slurry were deposited on 200 mesh copper grids covered with thin amorphous carbon films. TEM and SAED results were acquired at 200 kV. The surface charge ($\zeta$-potential) of the NPs was evaluated by electrophoretic mobility measurements in ultrapure water with a Litesizer 500 (Anton Paar, Austria).

The elemental chemical composition (Ca and P) was evaluated by inductively coupled plasma optical emission spectrometry (ICP-OES, Optima 7300DV from University of Málaga, SCAI). Firstly, 2 mL of ultrapure nitric acid was used to dissolve 20 mg of the powdered sample. Secondly, the mix was diluted up to 100 mL with ultrapure water. Three measurements of Ca and P contents were carried out each in triplicate. The corresponding emission wavelengths were 317.93 nm (Ca) and 213.62 nm (P).

### MeJ release kinetics in aqueous medium

The release kinetics of MeJ was monitored by UV-vis spectroscopy (Cary 100, Agilent Technologies, Santa Clara, CA, USA) at room temperature. 40 mg of ACP-MeJ or 85 mg of Ap-MeJ NPs were added to a quartz cuvette with 2 mL of ultrapure water. The absorbance at $\lambda$ = 291 nm was measured in a continuous manner for 30 minutes each until reaching the plateau. Cumulative release (%) is the accumulative percentage of released MeJ with respect to the $Q_{max}$. The measurements were performed in triplicate.

### Evaluation of the protection against thermal degradation

30 drops of 100 μL containing: i) Ap-MeJ (2 mM MeJ), ii) ACP-MeJ (2 mM MeJ), iii) MeJ (5 mM) mixed with 170 mg Ap NPs (Ap + MeJ), and iv) free MeJ (10 mM) were placed on a glass slide, simulating the drops deposited on the leaves after foliar application. The samples were kept at 50 °C for 24 hours. After that, the drops were collected with 5 mL of ultrapure water and kept in the dark up to 72 hours to ensure that MeJ was completely desorbed from the NPs. Then, the sample was centrifuged (12 000 rpm, 10 minutes) to remove the NPs and quantify the amount of MeJ remaining in solution by UV-vis spectroscopy. The ratio of protection (%) was calculated as $MeJ_{final}/MeJ_{initial} \times 100$. Each assay was performed in triplicate.

### Plant field experiments on vineyards

Field experiments were carried out on Monastrell (*Vitis vinifera* L.) grapevines from experimental vineyards of Jumilla (Murcia, Spain) grafted onto 1103-Paulsen rootstock and trained in a vertical trellis system. Vine rows were arranged N–NW to S–SE with between-row and within-row spacing of 3 × 1.25 m in a completely randomized block design, with 30 vines for each treatment and 10 vines for each replication. The Monastrell grapevines were sprayed with four treatments as follows: 1) aqueous solution of MeJ at a concentration of 10 mM (MeJ), 2) aqueous suspension of 3.6 g L$^{-1}$ ACP-MeJ (resulting in a total concentration of 1 mM in MeJ), 3) aqueous suspension of 7.8 g L$^{-1}$ Ap-MeJ (resulting in a total concentration of 1 mM in MeJ) and 4) aqueous solution of only Tween 80 (0.1% v/v, control) which was used as a wetting and dispersant agent in all treatments. Foliar applications (200 mL) were performed at veraison and one week later. This assay was carried out during 2020 season and climatological data are shown in the study by Gil-Muñoz *et al.*[25] Vinification was carried out using a traditional methodology according to Gil-Muñoz *et al.*[25] and analyses were measured at the end of alcoholic fermentation in triplicate.

### Total anthocyanins and tannins in wines

Total anthocyanins and tannins were measured by spectrophotometry using a 1600 Shimadzu UV-vis spectrophotometer (Shimadzu, Duisburg, Germany). Total anthocyanins were determined by adding 0.5 mL of wine to 20 mL of 0.1 N HCl and measuring the absorbance at 520 nm after 30 min.[28] Total tannins were measured using 50 μL of wine to which 600 μL of a methyl cellulose solution (0.04%) was added. Then, 400 μL of a saturated solution of ammonium sulphate and 800 μL of $H_2O$ were added. The mixture was centrifuged at 10 000 rpm for 5 minutes and the absorbance was measured at 280 nm.[29]

### Statistical analysis

Statistical comparisons were analysed with GraphPad Prism software (version 6.0) using one-way or two-way ANOVA and Bonferroni's *post hoc* test. When *p*-values are lower than 0.05 (*i.e.*, $p < 0.05$), differences in the obtained numerical results were considered statistically significant.

## Results and discussion

### Synthesis and characterization of as-synthesized nanoelicitors

Biomimetic calcium phosphate NPs were synthesized through a batch precipitation protocol in the presence of citrate and carbonate, two relevant components of bone apatite.[14,17] Citrate and carbonate stabilize the amorphous calcium phosphate (ACP) phase, which precipitates at the early stages. This transient precursor is then transformed into nanocrystalline apatite (Ap), the most thermodynamically

stable phase.[16] Thus, the (crystalline) structure of the nanomaterials, and the morphology, can be controlled with the maturation time and the temperature.[14,15,17] Herein, ACP NPs were precipitated at early maturation (5 minutes) at room temperature. Ap was instead obtained at longer maturation times (24 hours) and higher temperature (60 °C).

The two types of NPs (ACP and Ap) were then functionalized with MeJ through a previously optimized protocol.[24] The TEM micrograph of ACP-MeJ NPs (Fig. 1a) shows round-shaped NPs with diameters falling in the 10–20 nm range, in perfect agreement with the size of pristine ACP NPs synthesized through the same protocol.[17] The SAED pattern (inset Fig. 1a) along with the XRD pattern (Fig. S1†) confirmed the amorphous nature of the NPs, before and after MeJ adsorption.

On the other hand, the TEM micrograph of Ap-MeJ (Fig. 1b) shows elongated NPs with a length of around 20 nm and a width of around 5 nm (Fig. S2C, Table S1†). The SAED pattern (inset Fig. 1b) displays the typical reflections 002, 112 and 004 of hydroxyapatite at a $d$-spacing equal to 3.44, 2.75 and 1.72 Å, respectively (ASTM Card file No. 9-432). Rietveld analysis of the XRD patterns of Ap-MeJ (Fig. S2B†) confirmed that anisotropic (elongated) Ap nanocrystals were produced (Table S1†). Neither the morphology nor the size of Ap NPs was affected by MeJ adsorption (Table S1†).[14,15,17] Nevertheless, the crystal size slightly increased after the adsorption process, due to the fact that they remained 24 hours in aqueous solution (Fig. S2, Table S1†).

The chemical composition (Ca and P contents) of the NPs was scarcely affected by MeJ adsorption (Table 1). ACP and ACP-MeJ NPs have a Ca/P molar ratio close to 1.5, in agreement with the molecular formula of ACP $(Ca_3(PO_4)_2)$.[30] Conversely, Ap and Ap-MeJ presented a higher Ca/P molar ratio, close to 1.67, which fits with the molecular formula of stoichiometric hydroxyapatite $(Ca_5(PO_4)_3OH)$.[16] In both cases, neither Ca nor P contents were affected by MeJ adsorption (Table 1).

The successful MeJ adsorption was confirmed by FTIR, X-ray photoelectron spectroscopy (XPS) and $\zeta$-potential. Fig. 2a shows the FTIR spectra of ACP and Ap NPs before and after MeJ adsorption. The Ap and Ap-MeJ spectra show the characteristic phosphate vibrational bands of apatite ($\nu_4 PO_4$ at 561 and 602 cm$^{-1}$ and $\nu_3 PO_4$ at 1032, 1046 and 1087 cm$^{-1}$). These phosphate absorption bands are broader for ACP and ACP-MeJ due to the lack of long-range order.[14,24] The FTIR

**Table 1** Chemical composition and surface charge of the two nanosystems, before and after MeJ adsorption. Ca/P refers to the molar ratio

| Sample | Ca (wt%) | P (wt%) | Ca/P | $\zeta$-Potential (mV) |
|---|---|---|---|---|
| ACP | 14.7 ± 0.1 | 8.1 ± 0.1 | 1.41 ± 0.03 | −10.5 ± 0.1 |
| ACP-MeJ | 15.6 ± 1.3 | 8.8 ± 1.3 | 1.49 ± 0.13 | −6.2 ± 1.0 |
| Ap | 31.0 ± 0.9 | 14.7 ± 0.2 | 1.62 ± 0.03 | −21.6 ± 0.2 |
| Ap-MeJ | 31.9 ± 0.7 | 14.9 ± 0.8 | 1.66 ± 0.05 | −16.4 ± 2.2 |

spectra before and after MeJ adsorption were similar, confirming that the composition of ACP and Ap NPs was not affected by MeJ adsorption. The unique difference was the presence of a vibrational band at 1740 cm$^{-1}$ ascribed to carbonyl (ketone) groups of MeJ.[31] This band is more intense in the ACP-MeJ spectrum than that for Ap-MeJ, indicating that MeJ is bound to a larger extent on ACP in comparison to Ap. In fact, MeJ quantification by UV-vis spectroscopy revealed a higher MeJ loading capacity for ACP-MeJ (10.6 ± 0.5% wt) than for Ap-MeJ NPs (4.5 ± 1.1% wt) (Fig. 2b).

The XPS spectra of the survey scan of Ap and Ap-MeJ were quite similar (Fig. S3†), displaying the characteristic peaks of apatite: the Ca 1s, Ca 2p and Ca 2s, P 2p and P 2s.[32] The high-resolution P 2p and Ca 2p spectral lines in Ap and Ap-MeJ were identical (Fig. S3†). The unique difference between both XPS spectra was found in the C 1s peak, which is shifted to higher energies, due to the bonding of MeJ to the Ap surface (Fig. S3†).

The changes in surface charge of the NPs before and after the functionalization were also evaluated (Table 1). The $\zeta$-potential of ACP and Ap NPs before MeJ adsorption was −10.5 ± 0.1 mV and −21.6 ± 0.2 mV, respectively. The negatively charged carboxyl groups of citrate at the NP surface were the main responsible for the negative values. MeJ functionalization provided NPs with less negative surface charge, *i.e.* $\zeta$-potential of −6.2 ± 1.0 mV (ACP-MeJ) and −16.4 ± 2.2 mV (Ap-MeJ) (Table 1). To evaluate whether the reduction of MeJ loading of Ap-MeJ was associated with the more negative surface charge of Ap, in comparison to the ACP/ACP-MeJ samples, we modified the surface charge of Ap NPs. To
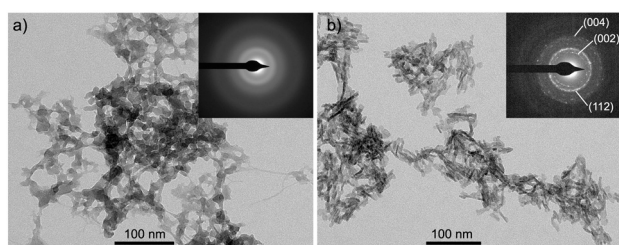


**Fig. 1** TEM images of ACP-MeJ (a) and Ap-MeJ (b). SAED patterns of the respective NPs are shown as an inset.
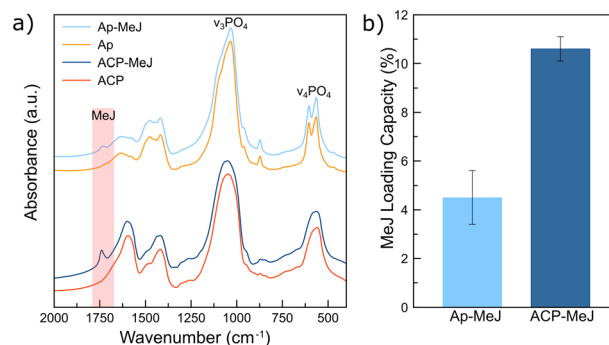


**Fig. 2** (a) FTIR spectra of Ap, ACP, Ap-MeJ and ACP-MeJ. (b) MeJ loading capacity of ACP-MeJ and Ap-MeJ NPs calculated by UV-vis spectroscopy.

this aim, the Ap NPs were immersed in sodium hydroxide solution to remove the citrate molecules from the NP surface. Ap* NPs with less negative surface charge ($-0.7 \pm 0.2$ mV, Table S2†) had a MeJ loading capacity of $6.9 \pm 0.4\%$ wt, slightly higher than that of Ap-MeJ ($4.5 \pm 1.1\%$ wt). This finding indicated that the surface charge has a very low impact on the loading capacity of calcium phosphate NPs. In contrast, other systems (*i.e.*, polymeric NPs) showed a more prominent effect of the surface charge on the encapsulation efficiency.[33] In this study, the highest MeJ content on ACP-MeJ compared to Ap-MeJ and Ap*-MeJ may be associated with the NP structure (amorphous *vs.* crystalline). ACP NPs have higher capacity to host exogenous ions or molecules (*e.g.*, citrate, urea, nitrate) than the crystalline apatite ones due to their short-range order.[17] The greater loading capacity of ACP is also associated with its higher surface reactivity and the presence of a high content of tightly bound water.[17,34] To this respect, ACP is more promising as nanocarriers of agrochemicals than Ap, even though the latter has been much more explored in the literature.[3,6]

### Release profile and *in vitro* MeJ protection effects

We evaluated the influence of the two types of calcium phosphate NPs, ACP-MeJ and Ap-MeJ, on the MeJ release kinetics in aqueous medium and MeJ degradation at high temperature. Fig. 3a shows a gradual and slow MeJ delivery from Ap-MeJ NPs which fits with a first order equation ($k = 0.051$ h$^{-1}$, $R^2 = 0.999$). The release rate of MeJ from Ap-MeJ is similar to the value for the ACP-MeJ one ($k = 0.045$ h$^{-1}$),[24] which reveals that neither crystallinity nor surface charge does affect the release rate of adsorbed molecules on their surface. On the other hand, the solubility of the adsorbates has a high impact on the release kinetics from calcium phosphate NPs. Whereas water-soluble molecules (*i.e.*, urea and nitrate) show a high release rate,[17] poor water-soluble adsorbates (*i.e.*, MeJ or doxorubicin) have a lower desorption

rate, similar to that of the calcium phosphate NP dissolution.[24,35]

We also evaluated the protective effect of the NPs against MeJ thermal degradation. To this aim, we measured the remaining MeJ concentration in drops of Ap-MeJ, ACP-MeJ and free MeJ after 24 hours at 50 °C by UV-vis spectroscopy (Fig. 3b). A solution containing free MeJ mixed with Ap NPs (Ap + MeJ) was also included. We observed no significant differences between the ACP-MeJ and Ap-MeJ samples, remaining in both cases more than 90% of the initial MeJ. This finding indicated that MeJ was protected by both types of NPs, regardless of their crystallinity, morphology or surface charge. On the other hand, free MeJ was almost degraded/evaporated after 24 hours. In the case of Ap + MeJ, only 25% of initial MeJ remained in the drops (Fig. 3b), confirming that our experimental protocol provides composite nanomaterials (ACP-MeJ or Ap-MeJ) with a higher level of performance in comparison to the sum of the parts (Ap + MeJ).

### Plant field experiments on Monastrell vineyards

The next step was evaluating the performance of the two types of NPs to efficiently deliver (and protect) the elicitor in plant field experiments on Monastrell red grapes (denomination of origin of Jumilla, Murcia). There is an ever-increasing interest in MeJ treatment in viticulture due to its effects on the synthesis of phenolic secondary metabolites in grapes, especially flavonol, anthocyanin, tannin and stilbene derivatives.[25] These metabolites help to define sensory characteristics of wines by contributing to their color, flavor and mouthfeel properties, aging potential, stability and beneficial health effects.[26,36] Most of the studies already reported were focused on the effects of the foliar application of 10 mM MeJ during veraison on the composition of most of the families of phenolic compounds in grapes and wines.[24–26]

In this work, we compared the composition of anthocyanins and tannins in wines from Monastrell grapes treated during veraison with 10 mM MeJ (positive control), Ap-MeJ (1 mM MeJ), ACP-MeJ (1 mM MeJ) and water as a control. Grapes treated with MeJ resulted in wines with a significant increase of the total anthocyanin concentration with respect to non-treated grapes (Fig. 4a). The anthocyanins are water-soluble pigments responsible for the red color and its tonality variations in grapes and red wines. These compounds also can contribute to the astringency and bitterness of grapes and wines.[26] Previous studies in *Vitis vinifera* L. Monastrell revealed that MeJ treatment (10 mM) increases the anthocyanin content of grapes and wines in two consecutive years (2009 and 2010).[20] It has been pointed out that jasmonic acid and MeJ are naturally occurring plant growth regulators that modulate chlorophyll degradation and anthocyanin biosynthesis.[20] However, ACP-MeJ and Ap-MeJ treatment did not enhance the anthocyanin content of wines with respect to the control (Fig. 4a).

More interestingly, both nanoparticle-based treatments enhanced the tannin concentration in wines with respect to
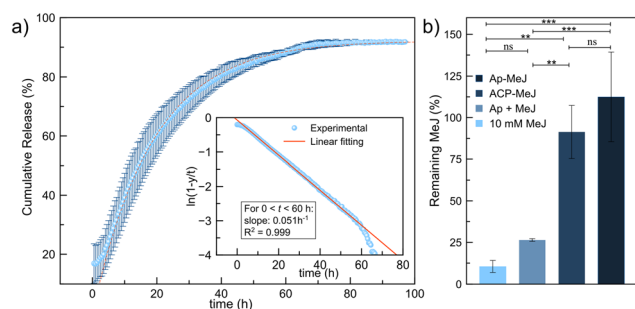


**Fig. 3** a) MeJ release profile from Ap-MeJ NPs in aqueous media. The dashed line represents the perfect experimental data fitting to a first order equation: $y(t) = a \times (1 - e^{-kt})$, where the rate constant $k = 0.051$ h$^{-1}$. b) Measurement of the remaining MeJ (%) in free MeJ dissolution, Ap + MeJ, ACP-MeJ and Ap-MeJ after 24 hours at 50 °C by UV-vis spectroscopy. Statically significant differences between measurements are marked with ** ($p$-value $< 0.01$) and *** ($p$-value $< 0.001$).
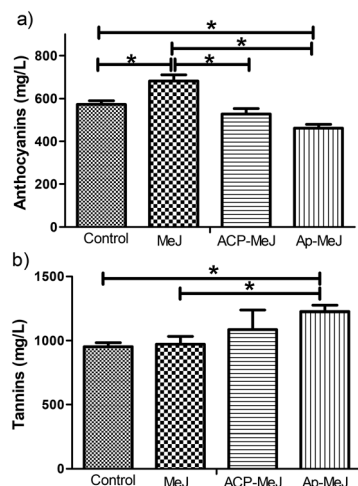
Fig. 4 Concentration (mg L$^{-1}$) of anthocyanins (a) and tannins (b) in wines from grapes treated with 10 mM free MeJ (MeJ) and 1 mM MeJ adsorbed into ACP (ACP-MeJ) and Ap (Ap-MeJ). Results of non-treated grapes (control) are also shown. Data are expressed as mean with their corresponding standard deviation as error bars. Statistically significant differences between measurements are marked with * (*p*-value < 0.05).

the control and free MeJ treatments (Fig. 4b), showing statistically significant differences only in Ap-MeJ treatment. Proanthocyanidins, commonly known as tannins, are flavonoid compounds found in grape skin and seeds. They play a relevant role in the organoleptic properties including wine mouthfeel, such as bitterness, hardness, dryness, astringency, structure, and body. Moreover, tannins participate in reactions with wine anthocyanins, favoring wine color stability with time.[20,27] It has been shown that premium Monastrell wines with high projected market prices are rich in tannins.[37] Gil-Muñoz et al. demonstrated that pre-harvest treatments with MeJ stimulated the production of tannins in both Tempranillo and Monastrell grapes and the corresponding wines, enhancing their quality and health-related properties.[20,27] However, they required ten times higher MeJ dosage (10 mM). In this work, we obtained similar results but at much reduced dosages using the NPs.

We can conclude that there were no significant differences between the two nanocarriers in the enhancement of anthocyanin and tannin contents in wine. Nonetheless, a recent study about the effect of the different MeJ treatments on the phenolic composition of the grape during the ripening period revealed a delayed effect of Ap-MeJ treatment on the increase of the anthocyanin content in the grape skin with respect to MeJ and ACP-MeJ treatments.[25] This delayed effect was most probably associated with the need for a greater Ap-MeJ uptake, at least twice that of ACP-MeJ, due to the lower MeJ content (Fig. 2b). At the harvest time, the three treatments showed similar improvement of anthocyanin and tannin contents in the grape skin.[25] Further experiments dedicated to track the fate of the NPs inside the plants are needed to evaluate the absorption mechanisms (and NP translocation) of the two types of NPs.

## Conclusions

Two types of calcium phosphate NPs are here compared as nanocarriers of methyl jasmonate, an elicitor extensively used in viticulture. Elongated apatite NPs, the most common calcium phosphate phase used in the agriculture field, were loaded with 4.5 wt% of MeJ affecting neither the NP morphology nor the structure. In contrast, amorphous NPs exhibited higher loading capacity (10.6 wt%). The study of the effect of surface charge revealed a slight increase of MeJ loading in less negative surface charge Ap NPs (6.9 wt%). Nonetheless, amorphous NPs present the highest MeJ content. ACP-MeJ and Ap-MeJ showed a gradual and slow release of MeJ with similar release rates (0.045 h$^{-1}$ and 0.051 h$^{-1}$, respectively) and almost identical protection action against thermal degradation. The efficiency of the NPs in delivering the elicitor was assayed by means of plant field experiments on Monastrell grapes. Wines from grapes treated with the two types of NPs showed similar anthocyanin and tannin contents, without significant differences between them. ACP-MeJ and Ap-MeJ treatments promoted the highest tannin concentration in wines, but they did not enhance the anthocyanin production with respect to the control treatment. Although the same MeJ concentration was applied for both nanosystems, the Ap-MeJ treatment required a nanoparticle concentration (7.8 g L$^{-1}$) double that of ACP-MeJ (3.6 g L$^{-1}$) due to its lower MeJ loading capacity. This finding is highly relevant for future application in the field since these less exploited calcium phosphate NPs allowed the required concentration of nanoelicitor to be reduced (and thus the associated production costs), with respect to Ap NPs, while maintaining the quality of the harvest.

## Author contributions

Conceptualization: J. M. D.-L., R. G.-M. and G. B. R.-R.; investigation: B. P.-T., M. S. F., M. J. G.-B., J. D. M.-O., J. A. B. S and D. F. P.-Q.; funding acquisition and supervision: J. M. D.-L. and R. G.-M.; writing – original draft: J. M. D.-L. and G. B. R.-R.; writing – review and editing: all the authors. All authors have read and agreed to the published version of the manuscript.

## Conflicts of interest

There are no conflicts to declare.

## Acknowledgements

## References

1 M. Usman, M. Farooq, A. Wakeel, A. Nawaz, S. A. Cheema, H. ur Rehman, I. Ashraf and M. Sanaullah, *Sci. Total Environ.*, 2020, **721**, 137778.

2 G. V. Lowry, A. Avellan and L. M. Gilbertson, *Nat. Nanotechnol.*, 2019, **14**, 517–522.

3 M. R. Al-Mamun, M. R. Hasan, M. S. Ahommed, M. S. Bacchu, M. R. Ali and M. Z. H. Khan, *Environ. Technol. Innovation*, 2021, **23**, 101658.

4 G. Fellet, L. Pilotto, L. Marchiol and E. Braidot, *Agronomy*, 2021, **11**, 1239.

5 C. Qi, S. Musetti, L.-H. Fu, Y.-J. Zhu and L. Huang, *Chem. Soc. Rev.*, 2019, **48**, 2698–2737.

6 G. Fellet, L. Pilotto, L. Marchiol and E. Braidot, *Agronomy*, 2021, **11**, 1239.

7 R. Liu, R. Lal and R. L. Ruiqiang Liu, *Sci. Rep.*, 2014, **4**, 5686.

8 N. Kottegoda, C. Sandaruwan, G. Priyadarshana, A. Siriwardhana, U. A. Rathnayake, D. M. Berugoda Arachchige, A. R. Kumarasinghe, D. Dahanayake, V. Karunaratne and G. A. J. Amaratunga, *ACS Nano*, 2017, **11**, 1214–1221.

9 M. R. Maghsoodi, L. Ghodszad and B. Asgari Lajayer, *Environ. Technol. Innovation*, 2020, **19**, 100869.

10 L. Xiong, P. Wang, M. N. Hunter and P. M. Kopittke, *Environ. Sci.: Nano*, 2018, **5**, 2888–2898.

11 A. S. Giroto, G. G. F. Guimarães, M. Foschini and C. Ribeiro, *Sci. Rep.*, 2017, **7**, 46032.

12 A. Adamiano, G. Fellet, M. Vuerich, D. Scarpin, F. Carella, C. Piccirillo, J. R. Jeon, A. Pizzutti, L. Marchiol and M. Iafisco, *Molecules*, 2021, **26**, 1–15.

13 C. Ma, Q. Li, W. Jia, H. Shang, J. Zhao, Y. Hao, C. Li, M. Tomko, N. Zuverza-Mena, W. Elmer, J. C. White and B. Xing, *Environ. Sci. Technol.*, 2021, **55**, 13465–13476.

14 J. M. Delgado-López, M. Iafisco, I. Rodríguez, A. Tampieri, M. Prat and J. Gómez-Morales, *Acta Biomater.*, 2012, **8**, 3491–3499.

15 J. M. Delgado-López, R. Frison, A. Cervellino, J. Gómez-Morales, A. Guagliardi and N. Masciocchi, *Adv. Funct. Mater.*, 2014, **24**, 1090–1099.

16 Y. Chen, W. Gu, H. Pan, S. Jiang and R. Tang, *CrystEngComm*, 2013, **16**, 1864–1867.

17 G. B. Ramírez-Rodríguez, G. Dal Sasso, F. J. Carmona, C. Miguel-Rojas, A. Pérez-De-Luque, N. Masciocchi, A. Guagliardi and J. M. Delgado-López, *ACS Appl. Bio Mater.*, 2020, **3**, 1344–1353.

18 M. Halder, S. Sarkar and S. Jha, *Eng. Life Sci.*, 2019, **19**, 880–895.

19 J. Zhao, L. C. Davis and R. Verpoorte, *Biotechnol. Adv.*, 2005, **23**, 283–333.

20 Y. Ruiz-Garcia, I. Romero-Cascales, R. Gil-Munoz, J. I. Fernandez-Fernandez, J. M. Lopez-Roca and E. Gomez-Plaza, *J. Agric. Food Chem.*, 2012, **60**, 1283–1290.

21 R. Gil-Muñoz, J. I. Fernández-Fernández, O. Crespo-Villegas, T. Garde-Cerdán, R. Gil-Munoz, J. I. Fernandez-Fernandez, O. Crespo-Villegas, T. Garde-Cerdan, R. Gil-Muñoz, J. I. Fernández-Fernández, O. Crespo-Villegas and T. Garde-Cerdán, *Food Res. Int.*, 2017, **98**, 34–39.

22 U. Hartmond, R. Yuan, J. K. Burns, A. Grant and W. J. Kender, *J. Am. Soc. Hortic. Sci.*, 2000, **125**, 547–552.

23 L. Chronopoulou, L. Donati, M. Bramosanti, R. Rosciani, C. Palocci, G. Pasqua and A. Valletta, *Sci. Rep.*, 2019, **9**, 1–9.

24 B. Parra-Torrejón, G. B. Ramírez-Rodríguez, M. J. Giménez-Bañón, J. D. Moreno-Olivares, D. F. Paladines-Quezada, R. Gil-Muñoz and J. M. Delgado-López, *Environ. Sci.: Nano*, 2021, **8**, 3524–3535.

25 R. Gil-Muñoz, D. F. Paladines-Quezada, M. J. Giménez-Bañón, J. D. Moreno-Olivares, J. A. Bleda-Sánchez, J. I. Fernández-Fernández, B. Parra-Torrejón, G. B. Ramírez-Rodríguez and J. M. Delgado-López, *Appl. Sci.*, 2023, **13**, 1906.

26 G. Gutiérrez-Gamboa, R. Mateluna-Cuadra, I. Díaz-Gálvez, N. Mejía and N. Verdugo-Vásquez, *Horticulturae*, 2021, **7**, 133.

27 R. Gil-Muñoz, J. I. Fernández-Fernández, J. Portu and T. Garde-Cerdán, *Eur. Food Res. Technol.*, 2018, **244**, 611–621.

28 R. Renard, P. Cottereau and L. Cayla, *Rev. Fr. Oenol.*, 2002, 10–16.

29 P. A. Smith, *Tech. Rev.*, 2005, **158**, 3–7.

30 S. V. Dorozhkin, *Acta Biomater.*, 2010, **6**, 4457–4475.

31 T. Sato, T. Kawara, K. Sakata and T. Fujisawa, *Bull. Chem. Soc. Jpn.*, 1981, **54**, 505–508.

32 V. Uskoković, *Phys. Chem. Chem. Phys.*, 2020, **22**, 5531–5547.

33 Y. Wang, P. Li and L. Kong, *AAPS PharmSciTech*, 2013, **14**, 585–592.

34 C. Combes and C. Rey, *Acta Biomater.*, 2010, **6**, 3362–3378.

35 J. M. Delgado-López, I. Rodríguez-Ruiz, M. A. Durán-Olivencia, M. Iafisco, A. Tampieri, D. Colangelo, M. Prat and J. Gómez-Morales, *Langmuir*, 2013, **29**, 8213–8221.

36 D. Pascual-Teresa, D. A. Moreno and C. García-Viguera, *Int. J. Mol. Sci.*, 2010, **11**, 1679–1703.

37 E. Gómez-Plaza, O. Olmos and A. B. Bautista-Ortín, *Food Chem.*, 2016, **204**, 506–512.